Ind. J. Pharm. Edu. Res., 2023; 57(4):1002-1011.
https://www.ijper.org

Original Article

Ameliorating the Poor Dissolution Rate of Selexipag in Aqueous Acidic Conditions Following Confinement into Mesoporous Silica

Mohamed S. Attia*, Fakhr-Eldin S. Ghazy

Department of Pharmaceutics, Faculty of Pharmacy, Zagazig University, Zagazig, EGYPT.

ABSTRACT

Background: Pulmonary Arterial Hypertension (PAH) is a serious condition with available treatment options, including Selexipag (SXP), a selective prostacyclin receptor agonist that has effectively reduced patient morbidity and mortality. SXP is limited by poor water solubility, especially in acidic solutions, which can affect its bioavailability and therapeutic efficacy. Therefore, strategies to tackle the solubility of SXP, such as nano-based Drug Delivery Systems (DDSs), should be explored. **Objectives:** The study aimed to tackle the poor dissolution rate of SXP and, consequently, improving the clinical efficacy and treatment outcomes of PAH patients. **Materials and Methods:** Three forms of Mesoporous Silica Nanoparticles (MSNs) were investigated as a DDS. SXP was loaded to MSNs (SBA-15, MCM-41, and KIT-6) via rotary evaporation technique and characterized for *in vitro* dissolution rates, drug release kinetics, morphology, crystallinity, interaction and surface properties. **Results and Conclusion:** Incorporating SXP as a monolayer to SBA-15 formulations significantly improved its dissolution rate, achieving an enhancement ratio of 9.48 at pH 1.2 compared to the pure drug. Notably, the monolayer and double-layer-loaded SBA-15 formulations exhibited the highest dissolution efficiency percentages, with values of 72.85% and 69.01%, respectively, surpassing that of raw SXP. The entrapment of SXP within SBA-15 mesopores was evident from pore volume reduction. The enhancement in dissolution rates was ascribed to the conversion of SXP into an amorphous state upon confinement within the nanostructure, which was indicated through X-ray diffraction and scanning electron microscopy analyses.

Keywords: Mesoporous silica, Drug dissolution, Selexipag, Solubility, Pulmonary arterial hypertension, Crystallinity.

Correspondence:
Mohamed S. Attia
Department of Pharmaceutics, Faculty of Pharmacy, Zagazig University, Zagazig-44519, EGYPT.
Email: msalahatia@zu.edu.eg; mosalahnabet@gmail.com;

Received: 14-01-2023;
Revised: 26-03-2023;
Accepted: 12-06-2023.

INTRODUCTION

The medical condition of Pulmonary Arterial Hypertension (PAH) is described as the presence of abnormally increased blood pressure in the pulmonary arteries.[1] A variety of FDA-approved treatment options are available for patients diagnosed with PAH. These agents include endothelin receptor antagonists, Phosphodiesterase-5 (PDE-5) inhibitors, and prostacyclins.[2] Selexipag (SXP) is a potent remedy for lessening morbidity and mortality in PAH patients. This drug is a selective prostacyclin receptor agonist with distinctive pharmacokinetic/pharmacodynamic properties from synthetic prostacyclins and their analogues, such as Iloprost and Beraprost.[3] Furthermore, SXP has an adequate safety profile and has the potential to be an appropriate treatment option for patients who have not responded to oral combination therapy with endothelin receptor antagonists and PDE-5 inhibitors.[4,5]

On the other hand, the delivery of this agent may be limited by the need for frequent inhalations or continuous intravenous or subcutaneous administrations. Additionally, SXP possesses low oral bioavailability of about 50% and a poor dissolution profile, posing clear constraints to both *in vitro* and *in vivo* performance. This is explained by the physicochemical nature of SXP, which is a highly permeable drug with low water solubility that is categorized as a class II drug by the Biopharmaceutics Classification System.[6] The solubility profile of SXP was reported to be pH dependent, exhibiting a high solubility in alkaline media while being insoluble in acidic conditions.[6]

In terms of patient convenience, effectiveness, patient-friendliness, and least invasiveness, the oral route is considered the most satisfactory, efficient, tolerant, and least invasive compared to other methods of drug administration.[7] In spite of these positive aspects, oral administration has several limitations, including the drug susceptibility to enzymes under different

DOI: 10.5530/ijper.57.4.122

enzymatic and pH conditions of the Gastrointestinal Tract (GIT), the challenges encountered in controlling drug release, and the low dissolution, absorption, and bioavailability of several drugs from the GIT.[8]

Nanoparticle systems have gained significant interest as drug carriers because of their ability to overcome the barriers of the GIT more effectively than other formulation strategies such as nanosized solid dispersion,[9,10] nanosuspension,[6] nanoliposomes,[11] nanoemulsion,[12] and nanomicelles.[13] Nanoparticles offer several advantages, including increased drug solubility, improved bioavailability, sustained drug release, and targeted drug delivery, making them an attractive option for drug development.[14] Furthermore, nanoparticle-based DDSs can be tailored to specific drug properties and patient needs, thereby improving treatment outcomes and patient compliance.

Recent reports have highlighted the efficacy of Mesoporous Silica Nanoparticles (MSNs) in overcoming the challenge of low bioavailability associated with poorly water-soluble pharmaceuticals when administered Orally.[15] As a drug delivery carrier, MSNs are chemically inert, and silica was deemed generally recognized as safe by the FDA.[16] Additionally, MSNs are recommended over the typical drug carriers in controlling the drug release,[17] owing to tremendous porosity and surface area, which permit them to confine higher drug amounts.[18] Florek *et al*., 2017 and Musallam *et al*., 2022 stated that drug confinement into MSNs nanopores changes the crystal habit to the amorphous states and consequently augments the drug solubility.[8,19] As well, the presence of the entrapped drug inside the MSN pores may deter its recrystallization process upon storage.[20] Herein, we aimed to investigate the effectiveness of three forms of MSNs as nanocarriers for SXP to increase its dissolution rate. The SXP was loaded onto MSNs using rotary evaporation and characterized for *in vitro* drug dissolution, dissolution kinetics, morphology, crystallinity, and interaction.

MATERIALS AND METHODS

SXP was supplied by Megafine Pharma Ltd., The mesoporous silica types MCM-41 (SA > 800 m^2/g), SBA-15 (SA= 550-600 m^2/g), and KIT-6 (SA = 600 m^2/g) were obtained from XFNANO Co., Ltd., China. Buffer components (Potassium Dihydrogen Orthophosphate and Disodium Hydrogen Orthophosphate) were purchased from El Nasr Pharmaceutical Chemicals Company, Egypt. Acetone was obtained from Thermo Fisher Scientific. All other chemicals used in this study were of analytical grade.

Drug loading calculations

To maximize drug loading, it is essential to efficiently utilize the MSNs' entire surface area. The maximum amount of SXP that can be loaded onto the carrier can be determined using the theoretical calculations of Dening and Taylor (2018) and Le *et al*. (2019).[21,22] The theoretical monolayer can be calculated by utilizing the specific surface area of the adsorbent (MSNs), the molecular weight of the adsorbate (SXP), the maximum exposed contact surface area of a single molecule of the drug, and Avogadro's number. The Cambridge Crystallographic Data Centre (CCDC) provides the data necessary to calculate the maximum exposed contact surface area of a single molecule, while the specific surface area of the MSNs is determined using the multipoint BET method. This calculation enables us to identify the optimal conditions for loading SXP onto MSNs and improve its dissolution rate.

$$TSCL = (\%\ W_{SXP} / W_{MSN}) = \frac{SSA \times M_w \times 10^{20}}{SA_M \times N_A}$$

Where, SSA represents the specific surface area of the adsorbent (mesoporous silica) in square meters per gram. Mw refers to the molecular weight of SXP in grams per mole. SA_M stands for the maximum exposed contact surface area of a single molecule in square angstroms, which is calculated based on the two largest molecular dimensions of the molecule (37.96 and 22.47 Å). N_A represents Avogadro's number, which is 6.022 × 10.[23] The data required for the calculation of SA_M were obtained from CCDC under deposition number 1892239.

Loading MSNs with SXP

A rotary evaporation technique was utilized for loading MSN formulations, which has been reported by Budiman and Aulifa (2021) as an effective method for incorporating different drugs into mesoporous silica.[23] A concentrated solution of SXP (10 mg/mL) in acetone was prepared. Aliquots of this solution were then mixed with a specific quantity of porous silica, resulting in various drug saturation levels through the formation of mono-and double-layered MSNs. The resulting mixture was transferred to a rotary evaporator flask and subjected to ultrasonication for 5 min and vortexed for 10 min to disperse any silica aggregates. The SXP-MSNs dispersion in acetone was then left to evaporate under vacuum via Heidolph rotary evaporator (40°C, 100 rpm).

Characterization of SXP-loaded MSNs

In vitro dissolution studies

The dissolution characteristics of SXP from MSN formulations were evaluated using a USP dissolution apparatus II.[24] Pure SXP (5 mg) and equivalent amounts of MSNs formulations were added to 500 mL of aqueous media containing 0.5 M phosphate buffer (pH = 5.8) and 0.1N HCl (pH = 1.2) in the dissolution vessel, and the paddle speed was set at 100 rpm while maintaining a temperature of 37 ± 0.5°C to simulate physiological conditions. Samples were collected at predetermined intervals (5, 10, 20, 30, 40, 50, and 60 min) and centrifuged at 7000 rpm for 5 min to remove any suspended particles. The same withdrawn volume of

fresh dissolution medium was added to retain sink conditions.[25] The samples were then analyzed at λ_{max} of 299 nm using spectrophotometry to quantitatively determine the drug content. The measurements were performed in triplicate, and the results were reported as mean ± standard deviation.

Drug dissolution comparisons and kinetics analysis

Drug dissolution kinetics and dissolution parameters such as Mean Dissolution Time (MDT), Dissolution Efficiency percentage (DE%), Enhancement Ratio (ER), f_1 (Difference Factor), and f_2 (Similarity Factor) were evaluated using DDSolver.xla software following the methodology outlined in previously published articles.[26,27]

Scanning Electron Microscope (SEM)

SEM was employed to investigate the external morphology of both raw SXP and SXP-loaded SBA-15. The samples were prepared by spreading a thin layer of the materials on double-sided carbon adhesive tape and treated under a high vacuum to prevent electron charging during imaging.[28] Detailed images were captured using a scanning electron microscope (JEOL-JSM-6510LV, Tokyo, Japan) to provide a comprehensive understanding of the external morphology of the samples.

Fourier Transform Infrared (FTIR) Spectroscopy

To explore the potential bonding between SXP and the excipients, a comparison was carried out between the FTIR spectra of the pure SXP powder, untreated silica, and the chosen PMs and MSNs formulations. The FTIR spectra were acquired using Nicolet iS10 FTIR spectrometer (Thermo Fisher Scientific, Massachusetts, USA). The potassium bromide disc method was used with a scanning range of 400–4000 cm^{-1}.[29]

Powder X-ray Diffraction (PXRD)

A thorough PXRD analysis was conducted to examine the solid state of SXP in the selected SXP-loaded silica formulation. The analysis was carried out using an X-ray diffractometer (D2 Phaser, Bruker, Massachusetts, USA) at room temperature, utilizing monochromatic Cu Kα radiation (l = 1.5406 Å) at 30 mA and 40 kV. The X-ray diffraction pattern was recorded in the 2θ range of 5° to 50° with an angular increment of 0.02° per second. This technique facilitated the detection of any alterations in the crystal structure of SXP and the identification of any potential amorphous regions present in the formulation, providing an extensive understanding of the solid-state properties of the entrapped drug.[30]

Surface analysis

Nitrogen adsorption-desorption isotherms analysis was conducted to determine the surface properties of untreated SBA-15 and SXP-loaded SBA-15. The samples were degassed overnight at 60°C to remove adsorbed gases before measurements. The BELSORP-miniX gas sorption analyzer (S/N: 10039, Version 1.1.3.1) was used at 77.35 K to precisely determine the surface area, pore volume, and pore size distribution of the samples. This method offers a detailed understanding of the textural characteristics of the materials and their potential impact on drug loading and release properties. Data were analyzed via BELMaster software (Version 7.3.2.0).

The pore volume and diameter distribution were determined using Non-Local Density Functional Theory (NLDFT/GCMC) and Barret-Joyner-Halenda (BJH) adsorption models, and the results were compared.[31] Meanwhile, the specific surface area of the mesoporous silica was determined using the multipoint BET method, based on isotherm adsorption data at P/P0 from 0.05 to 0.30, following the method described by Huang *et al.* (2014).[32]

RESULTS AND DISCUSSION

Drug loading optimization

To achieve the optimal loading SXP to the nanopores of MSNs, the TSCL was calculated using the molecular weight of SXP and molecular dimensions obtained from the CCDC database, along with the surface area for each type of MSN. Since the surface area for MCM-41 was approximately double that of SBA-15 and KIT-6, the SXP monolayer loading percentage was 10.5, 5.7, and 5.5 % (w/w) for MCM-4, SBA-15, and KIT-6, respectively (Table 1).

In vitro drug release

The observed *in vitro* drug dissolution rates were presented in Figure 1, where all SXP-loaded MSN formulations have significantly improved the dissolution rate compared to naïve SXP. The dissolution patterns of SXP from KIT-6, SBA-15 and MCM-41 were compared to the pure crystalline SXP in two dissolution media: 0.1N HCl (pH 1.2) and phosphate buffer (0.05M, pH 5.5). It was evident that about 25 and 15% of raw SXP were dissolved after passing 1 hr in phosphate buffer and HCl, respectively, which implied the limited solubility of SXP. The loaded monolayer of SXP to MSNs surface was found to have the fastest dissolution at 5 min compared to the higher saturation level with a short MDT at pH 5.8 and 1.2 (MDT = 7.82 and 4.89 min, respectively) (Table 2). This was attributed to the change in SXP crystallinity when confined in the nanosized pores of the mesoporous structure, resulting in a more soluble amorphous state of SXP.[22,33,34] At pH 5.8, the monolayer and double layer of SXP-loaded SBA-15 exhibited the highest dissolution efficiency percentage (72.85 and 69.01, respectively) compared to raw SXP (15%). Meanwhile, at pH 1.2, the monolayer of SXP-loaded-loaded SBA-15 formulation exhibited an improved dissolution rate of SXP, with an enhancement ratio of 9.48 compared to the pure drug. Subsequently, the release of SXP from double-layer loaded SBA-15 and MCM-41 was enhanced at 45 min, which could be ascribed to the reversible adsorption phenomenon. This

phenomenon involves silica adsorption to the drug, hindering the release of the unreleased SXP owing to silica content in the formulation.[22] The silica content in the mono-layer SBA-15 formulation, which was about 94%, can account for the perceived decrease in the release rates at these time points. However, KIT-16 showed a lower dissolution rate than the abovementioned MSNs at both saturation levels with relatively low f_1 values (152.9 and 144.9), respectively.

Drug dissolution kinetics

The dissolution profiles were tested for fitting to the mathematical models, including zero-order, first-order, Higuchi, Korsmeyer-Peppas, and rate constants (k) for pure SXP, and the MSNs formulations were determined and reported in Tables 3 and 4. The decision on the release model was based on the regression parameters (R2 and AIC); therefore, the criteria for model selection is based on the lowest AIC and highest coefficient of determination values to confirm the goodness of fit.

The dissolution profile of pure SXP showed fitting to the linear first-order kinetic models in both dissolution media, with R^2 reaching up to 0.99 with increasing acidity of the media. This was confirmed by the Korsmeyer-Peppas result with a diffusion coefficient (n) = 0.66, which implies that SXP followed a first-order or pseudo-first-order kinetic and indicates the presence of boundaries affecting passive drug diffusion.

In contrast, the dissolution pattern of loaded silica formulations depended on the MSNs type, which might be affected by the mesoporous structure. SBA-15 and MCM-41 have similar hexagonal symmetry, whereas KIT-6 has bicontinuous cubic mesostructured with Ia3d symmetry. The change in MSNs symmetry might explain the variation SXP release pattern, thereby affecting the kinetics of drug dissolution. At pH 5.8, KIT-6 showed a closely fitted release profile to the Higuchi model with a coefficient of determination = 0.96, 0.98 for monolayer and double-layer loaded KIT-6, respectively.

Furthermore, typical drug release models such as zero-, first-order, and Higuchi have failed to describe the dissolution profiles of SXP-loaded SBA-15 and MCM-41 at both drug loading levels. On the contrary, the model of Korsmeyer-Peppas showed high goodness of fit since it showed a high correlation (>0.99), and AIC favoured Korsmeyer-Peppas. The n values retrieved from Korsmeyer's model for all SXP-loaded MSNs were below 0.5, which is a typical Fickian diffusion, implying the absence of boundaries that shape the passive diffusion process. According to the Korsmeyer-Peppas model, it was anticipated that the time required to release 90% of the drug (T_{90}) from raw SXP would be

Table 1: The loading of SXP in MSNs expressed as a weight-to-weight percentage.

Saturation level	Silica type		
	MCM-41	SBA-15	KIT-6
Monolayer loading (100% Saturation)	10.5%	5.7%	5.5%
Double layer loading (200% Saturation)	21.1%	11.4%	11.1%

Table 2: Dissolution parameters of SXP and SXP-Loaded MSNs formulations in phosphate buffer (pH 5.8, 0.05M) and HCl (pH 1.2, 0.1N).

Dissolution model	SXP	KIT-6		SBA-15		MCM-41	
At pH 5.8	Saturation level						
		100%	200%	100%	200%	100%	200%
MDT (min)	24.36	18.58	19.30	7.82	24.36	11.45	10.14
ER	--	2.547	2.47	4.85	4.59	4.215	4.03
DE (%)	15.01	38.24	37.11	72.85	69.01	63.28	60.58
f_1	--	152.95	144.94	371.77	348.38	308.38	292.82
f_2	--	31.83	32.91	12.69	14.10	16.75	17.79
At pH 1.2							
MDT (min)	26.94	10.45	13.12	4.89	6.65	8.89	12.47
ER	--	3.96	3.78	9.48	9.35	6.03	5.74
DE (%)	8.67	34.36	32.85	82.28	81.14	52.30	49.86
f1	--	248.06	238.74	692.70	691.07	421.45	405.24
f2	--	30.50	31.35	8.23	8.29	19.02	19.84

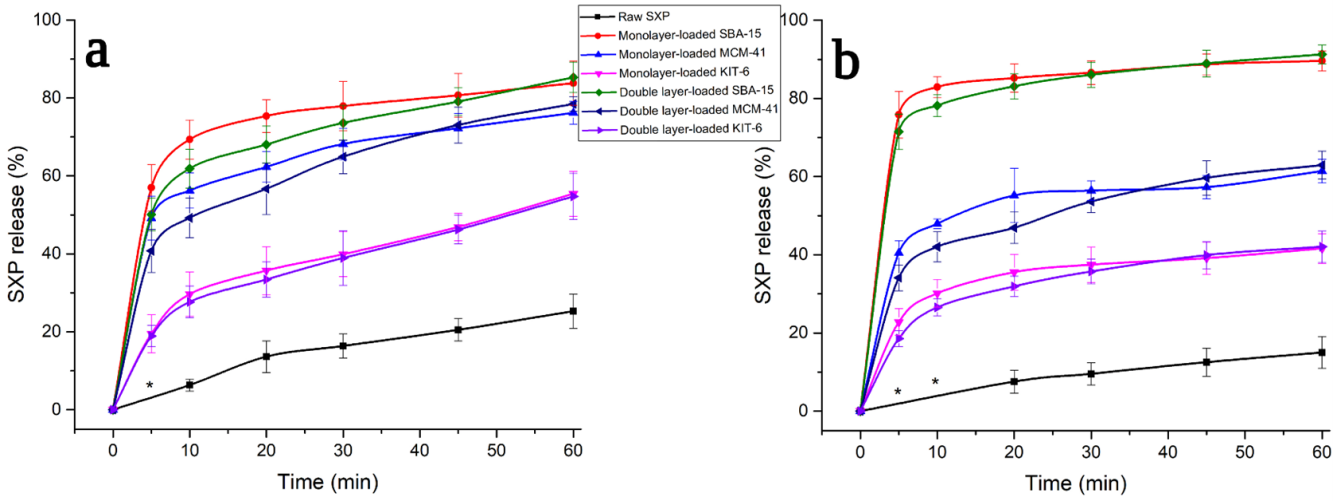

Figure 1: *In vitro* drug release from raw SXP and SXP-loaded MSNs in dissolution media of (a) 0.05M phosphate buffer (pH 5.8) and (b) 0.1N HCl (pH 1.2). Asterisk (*) indicates that SXP concentration was not measurable.(*) indicates that SXP concentration was not measurable.

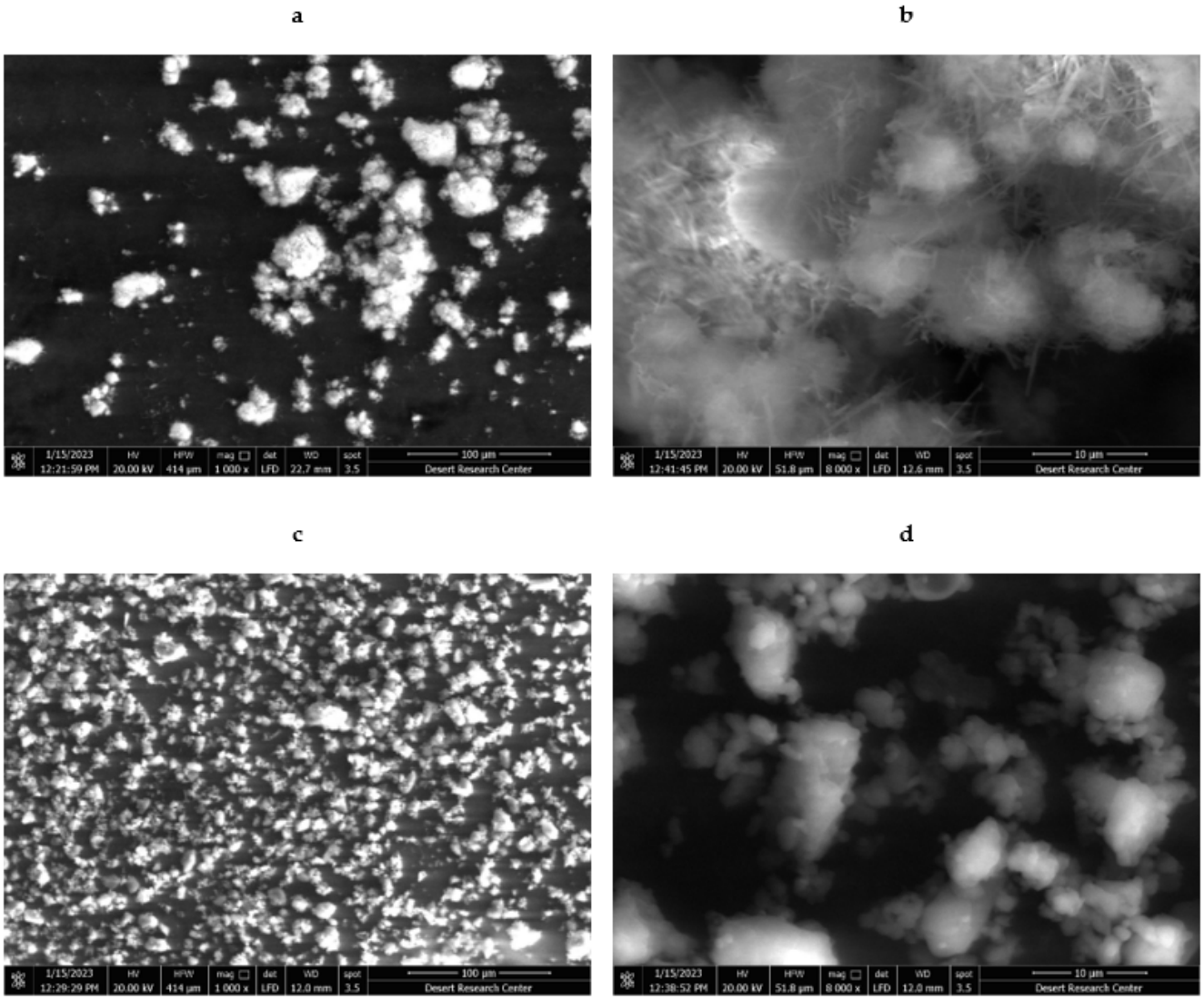

Figure 2: SEM images of raw SXP (a, c) and SXP-loaded SBA-15 (b, d) at magnifications of 1000x (a, c) and 8000x (b, d), respectively.

approximately 405 and 554 min at pH 5.8 and 1.2, respectively. However, loading SXP as a double-layer onto SBA-15 reduced the T_{90} values (81 and 45 min at the same pH values, respectively).

Morphology analysis (SEM)

Microscopical analysis revealed that the SXP crystals were mostly in the micrometre range and possessed fibers embedded into SXP particles, as depicted in (Figure 2 a,b). This fibrous structure is likely a result of the parallel alignment of the crystal molecules during growth. It is worth noting that this fibrous structure may impact the physical properties and biological behavior of SXP, such as affecting its dissolution rate and bioavailability.

In contrast, the loaded MSNs did not exhibit any fibrous structure, as seen in the overview of the samples (Figure 2 c,d). This suggests that the SXP molecules could not form the same crystal structure when entrapped within the silica nanoparticles. It is possible that the smaller size and varying surface properties of the MSNs hindered the formation of the fibrous crystal structure observed in the micrometre-sized crystals. This could be explained by the entrapment of SXP within the mesoporous structure of the nanoparticles.

X-ray Powder Diffraction (XRPD)

The XRD study was conducted to ensure the complete confinement of the crystalline SXP in MSN-loaded formulations. Monolayer-loaded formulations were anticipated to present no change in the amorphous halopattern of blank MSNs. Figure 3 displays the XRD pattern of raw SXP and the untreated and treated MSNs, respectively. The XRD pattern of untreated SXP exhibited sharp and intense peaks at 2θ of 9.88, 15.69, 17.39, 19.72, 21.67, and 23.19, implying its crystallinity. These results align with Alwan *et al.*'s study, which demonstrated a similar XRD pattern of SXP.[35] As can be seen in Figure 1, the materials SBA-15, MCM-41, and KIT-6 did not exhibit any distinct diffraction peaks associated with crystallinity, rather exhibiting a halopattern. These findings imply that these materials may possess an amorphous or disordered structure. Similar patterns were observed when these materials were loaded with SXP at 100% saturation, suggesting that crystalline forms of the drug are not present on the surface of the MSNs. Accordingly, the calculations for loading drugs onto the MSNs provided sound predictions of the SXP amount required to saturate the MSNs' surface with no further precipitation.

FTIR

Absorbance spectra of pure SXP powder, SBA-15, their physical mixture, and SXP-loaded SBA-15 are shown in Figure 4. In addition, reduced intensity, disappearance, or shifting peaks in any spectrum were studied to investigate the possible interaction of the physically mixed additive and formulated MSNs. The characteristic peak of SXP appeared as a weak absorption peak corresponding to the secondary N-H group at 3025 cm^{-1}. Stretching vibrations at 1595 and 1481 have indicated the aromatic C=C stretching. It can be seen in Figure 4a that a strong peak at 1118 cm^{-1} corresponds to C-N stretching, whereas the peak at 1725 corresponds to C=O of amide. Our reported results align with Villalva *et al.*[36] Nonetheless, SBA-15 showed an asymmetric stretching vibration Si-O-Si band that previously had been observed in the range of 1020-1080 cm^{-1}, as reported by Voycheva *et al.*[37] The peaks corresponding to Si-O-Si of SBA-15 were observed at 1073 (Figure 4b). A similar pattern was seen in the physical mixture to the untreated SBA-15 since it was present in a high concentration, approximately 95%. Figure 4c shows that no meaningful interaction has been detected since no characteristic peaks have disappeared or appeared. Only the peak appearing at 1068 exhibited an increased intensity, possibly due to the cumulative effect of C-N stretching of SXP and Si-O-Si stretching. On the other hand, in the loaded SBA-15 preparation, the Si-O-Si peak was shifted to 1062, and the intensity was reduced, as shown in the stacked Figure 4. This suggests a possible hydrogen bonding between the secondary amine of SXP and silanol groups of SBA-15 (Figure 4d).

Surface analysis

The full isotherm of SBA-15 and SXP monolayer-loaded SBA-15 was presented in (Figure 5a,b). According to the IUPAC classification, the isotherms can be categorized as form IV isotherms, which indicates the open mesopore of the investigated silica (SBA-15).[38,39] Moreover, the hysteresis loop (H1) appears at relative pressure (P/P_0) = 0.6 to 0.9, which is a characteristic feature of SBA-15 (Figure a).[40] The NLDFT/GCMC model was used to emphasize the results of pore size and pore volume since there were reports about the inaccuracy of the BJH model for measuring pore volume when the diameter is less than 10 nm.[41] The calculated data of surface area, pore volume, and pore diameter are presented in Table 5.

The pore volume of SXP-loaded SBA-15 was slightly reduced, as reported by the two models compared to blank SBA-15,

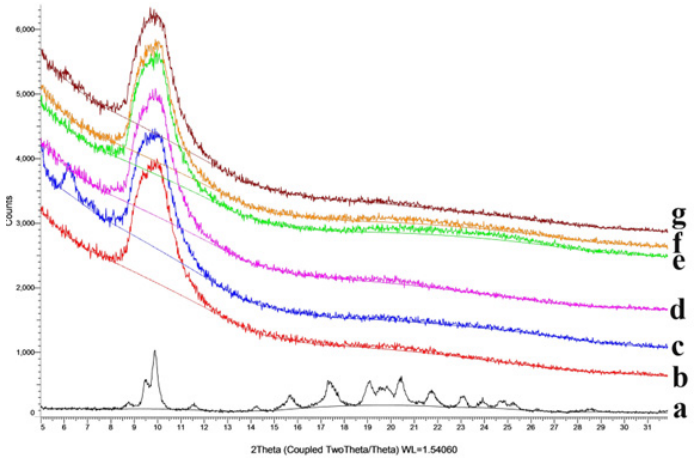

Figure 3: XRPD diffractograms of raw SXP (a), unloaded SBA-15 (b), MCM-41 (c), KIT-6 (d), and SXP-loaded SBA-15 (e), MCM-41 (f), KIT-6 (g).

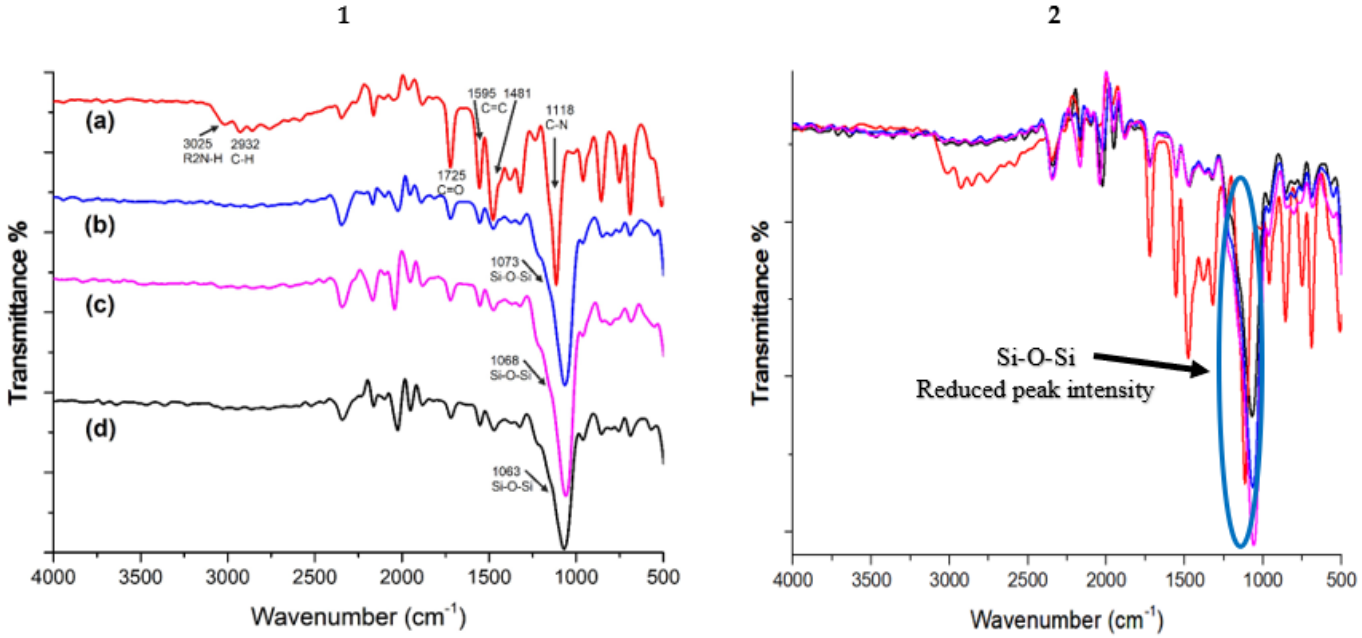

Figure 4: (1) FTIR spectra of SXP (a), unloaded SBA-15 (b), physical mixture (c), SXP-loaded SBA-15 (d). (2) Stacked spectra of SXP (red), unloaded SBA-15 (violet), physical mixture (blue), and SXP-loaded SBA-15 (black).

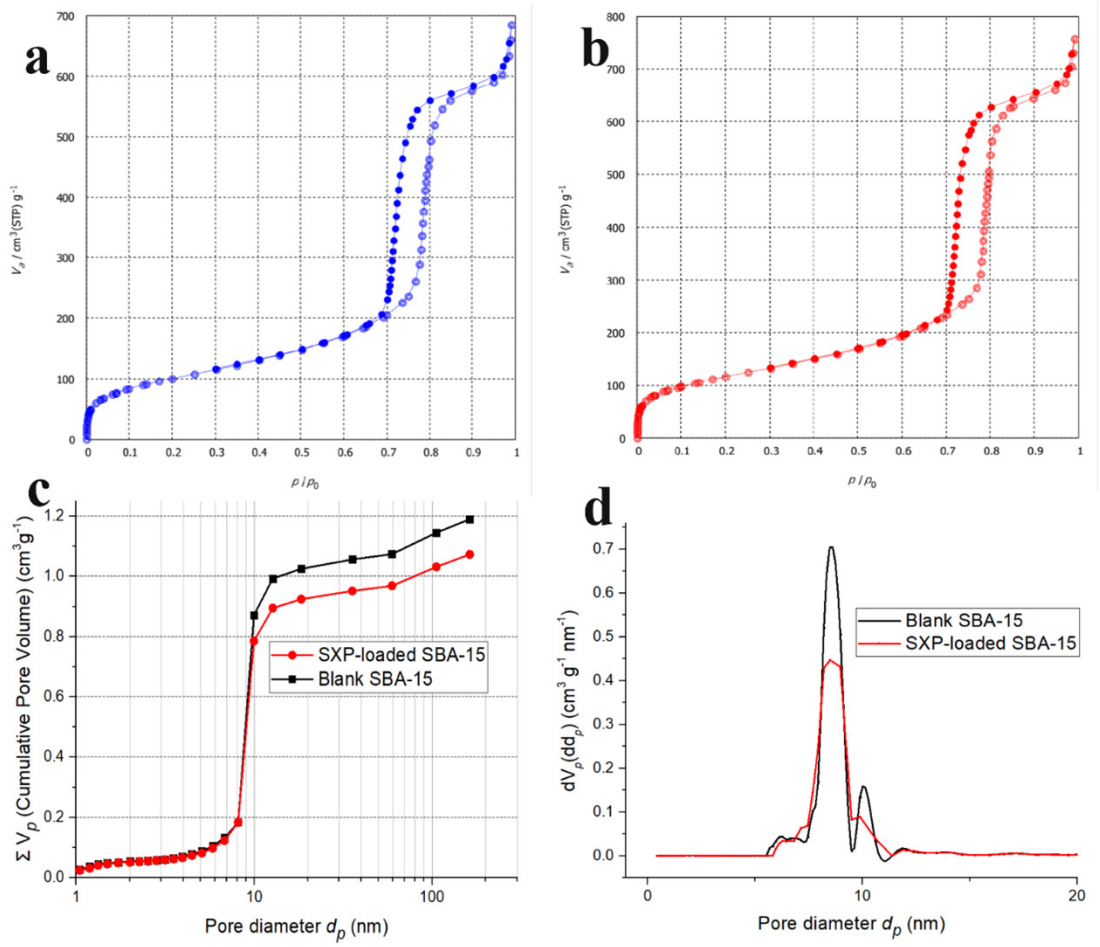

Figure 5: Complete N2 adsorption-desorption isotherm of (a) blank SBA-15 and (b) SXP-loaded SBA-15 (monolayer). Pore size distribution analysis by (c) BJH adsorption model and (d) NLDFT/GCMC model.

Table 3: Dissolution kinetic modelling for raw SXP and SXP-loaded MSN formulations in phosphate buffer (pH 5.8, 0.05M).

Dissolution model	SXP	KIT-6		SBA-15		MCM-41	
Saturation level		100%	200%	100%	200%	100%	200%
1-Zero-order							
K_O	0.46	1.09	1.07	1.91	1.86	1.69	1.67
R^2	0.92	0.55	0.61	-0.46	-0.11	-0.23	0.19
AIC	23.18	49.59	48.40	64.51	62.31	61.58	58.80
2-First-order							
K_1	0.005	0.017	0.01	0.105	0.06	0.05	0.04
R^2	0.95	0.76	0.79	0.73	0.74	0.56	0.74
AIC	20.27	45.30	44.00	52.43	51.97	54.30	50.79
3-Higuchi							
K_H	3.05	7.40	7.21	13.53	12.97	11.84	11.49
R^2	0.96	0.96	0.98	0.57	0.74	0.68	0.86
AIC	17.79	31.31	27.65	55.86	52.08	51.96	46.19
4-Korsmeyer-Peppas							
K_{KP}	1.67	11.25	10.04	48.51	37.64	37.31	26.25
n	0.66	0.38	0.40	0.13	0.19	0.17	0.26
R^2	0.99	0.99	0.99	0.99	0.99	0.99	0.99
AIC	12.58	22.63	19.75	27.41	20.31	5.15	13.73
T_{90} (min)	405.51	228.62	217.76	101.32	81.27	91.03	155.91

Table 4: Dissolution kinetic modelling for raw SXP and SXP-loaded MSN formulations in dissolution media containing 0.1N HCl (pH 1.2)

Dissolution model	SXP	KIT-6		SBA-15		MCM-41	
Saturation level		100%	200%	100%	200%	100%	200%
1-Zero-order							
K_O	0.27	0.92	0.90	2.11	2.10	1.38	1.36
R^2	0.98	-0.075	0.28	-0.88	-0.68	-0.38	0.10
AIC	7.46	52.44	49.74	67.67	66.77	59.61	56.64
2-First-order							
K_1	0.003	0.013	0.01	0.23	0.19	0.02	0.02
R^2	0.99	0.232	0.52	0.88	0.87	0.23	0.54
AIC	4.7	50.084	46.93	47.95	48.33	55.40	51.80
3-Higuchi							
K_H	1.84	6.44	6.21	15.15	15.01	9.75	9.41
R^2	0.98	0.760	0.90	0.32	0.44	0.61	0.83
AIC	3.55	41.94	36.01	60.45	58.94	50.68	44.91
4-Korsmeyer-Peppas							
K_{KP}	0.63	17.77	12.71	70.28	62.15	33.39	23.2
n	0.78	0.21	0.29	0.06	0.09	0.15	0.24
R^2	0.99	0.99	0.99	0.99	0.99	0.99	0.99
AIC	-3.57	21.39	18.51	18.57	9.16	23.65	14.23
T_{90} (min)	554.13	2045.42	702.11	56.24	49.55	734.96	254.01

Table 5: BET surface area, pore volume, and diameter of the untreated SBA-15 and SXP-loaded SBA-15.

Sample name	SABET (m2. g-1)	Pore volume ($cm^3. g^{-1}$)		Pore diameter (nm)	
		BJH Ads	NLDFT	BJH Ads	NLDFT/GCMC
Untreated SBA-15	589.55	1.19	1.11	7.95	8.78
SXP-loaded SBA-15	536.81	1.07	1.01	7.83	8.58

indicating successful entrapment of a small amount of SXP in the pores. Results of BJH and NLDFT/GCMC models confirmed a reduction in the pore volume of SBA-15 after drug loading by 10 and 9%, respectively. SBA-15 had a surface area of 589.55 m^2/g, as calculated by BET equations, and loading SXP led to reduced nitrogen adsorption to the SBA-15 nanopores, leading to an approximately 8.8% reduction in the total surface area, as shown in Table 5. Additionally, the pore diameters were around 8 nm, and SXP loading did not exert a noticed change in pore diameter, as seen in Figure 5d.

CONCLUSION

The present study provides compelling evidence for the prospective of MSNs to ameliorate the therapeutic efficacy of SXP in treating PAH. By serving as nanocarriers, MSNs have effectively improved the dissolution rate of SXP, with the monolayer SXP-loaded SBA-15 formulation demonstrating the most significant improvement. The successful entrapment of SXP within the nanopores of SBA-15 was demonstrated through the observed reduction in pore volume and disappearance of XRD peaks in the loaded formulations. Furthermore, the study showed that the amorphous state of SXP within MSNs did explain the notably observed improvement in dissolution rate. These findings indicate that MSNs show promise as a drug delivery system for SXP and further research is needed to evaluate the *in vivo* performance and the clinical application of MSNs for oral delivery of SXP.

ACKNOWLEDGEMENT

This paper is based upon work supported by Science, Technology and Innovation Funding Authority (STIFA) under Grant number 44758.

CONFLICT OF INTEREST

The authors declare no conflict of interest.

REFERENCES

1. Ogo T, Shimokawahara H, Kinoshita H, Sakao S, Abe K, Matoba S, et al. Selexipag for the treatment of chronic thromboembolic pulmonary hypertension. Eur Respir J. 2022;60(1). doi: 10.1183/13993003.01694-2021, PMID 34824052.
2. Delcroix M, Howard L. Pulmonary arterial hypertension: the burden of disease and impact on quality of life. Eur Respir Rev. 2015;24(138):621-9. doi: 10.1183/16000617.0063-2015, PMID 26621976.
3. Genecand L, Wacker J, Beghetti M, Lador F. Selexipag for the treatment of pulmonary arterial hypertension. Expert Rev Respir Med. 2021;15(5):583-95. doi: 10.1080/17476348.2021.1866990, PMID 33382345.
4. Coghlan JG, Picken C, Clapp LH. Selexipag in the management of pulmonary arterial hypertension: an update. Drug Healthc Patient Saf. 2019;11:55-64. doi: 10.2147/DHPS.S181313, PMID 31496830.
5. Panagiotidou E, Boutou A, Pitsiou G. An evaluation of selexipag for the treatment of pulmonary hypertension. Expert Opin Pharmacother. 2021;22(1):29-36. doi: 10.1080/14656566.2020.1812579, PMID 32867545.
6. Alwan RM, Rajab NA. Nanosuspensions of selexipag: formulation, characterization, and *in vitro* evaluation. Iraqi J Pharm sci P-ISSN. 1683;3597 E-ISSN:2521-3512. 2021;30(1):144–53.
7. Soares S, Costa A, Sarmento B. Novel non-invasive methods of insulin delivery. Expert Opin Drug Deliv. 2012;9(12):1539-58. doi: 10.1517/17425247.2012.737779, PMID 23098366.
8. Florek J, Caillard R, Kleitz F. Evaluation of mesoporous silica nanoparticles for oral drug delivery–current status and perspective of MSNs drug carriers. Nanoscale. 2017;9(40):15252-77. doi: 10.1039/c7nr05762h, PMID 28984885.
9. Attia MS, Elshahat A, Hamdy A, Fathi AM, Emad-Eldin M, Ghazy FS, *et al.* Soluplus® as a solubilizing excipient for poorly water-soluble drugs: recent advances in formulation strategies and pharmaceutical product features. J Drug Deliv Sci Technol. 2023;84:104519. doi: 10.1016/j.jddst.2023.104519.
10. Attia MS, Hasan AA, Ghazy FES, Gomaa E. Solid dispersion as a technical solution to boost the dissolution rate and bioavailability of poorly water-soluble drugs. Indian J Pharm Educ Res;55(3):13.
11. Lee MK. Liposomes for enhanced bioavailability of water-insoluble drugs: *in vivo* evidence and recent approaches. Pharmaceutics. 2020;12(3):264. doi: 10.3390/pharmaceutics12030264, PMID 32183185.
12. Ibrahim TM, Abdallah MH, El-Megrab NA, El-Nahas HM. Upgrading of dissolution and anti-hypertensive effect of carvedilol via two combined approaches: self-emulsification and liquisolid techniques. Drug Dev Ind Pharm. 2018;44(6):873-85. doi: 10.1080/03639045.2017.1417421, PMID 29254384.
13. Ke Z, Shi J, Cheng Z, Cheng X, Wang H, Wang M, *et al.* Design and characterization of gambogic acid-loaded mixed micelles system for enhanced oral bioavailability. Pharm Dev Technol. 2022;27(6):695-701. doi: 10.1080/10837450.2022.2107012, PMID 35899462.
14. Alqahtani MS, Kazi M, Alsenaidy MA, Ahmad MZ. Advances in oral drug delivery. Front Pharmacol. 2021;12:618411. doi: 10.3389/fphar.2021.618411, PMID 33679401.
15. Sreeharsha N, Philip M, Krishna SS, Viswanad V, Sahu RK, Shiroorkar PN, *et al.* Multifunctional mesoporous silica nanoparticles for oral drug delivery. Coatings. 2022;12(3):358. doi: 10.3390/coatings12030358.
16. Ghaferi M, Koohi Moftakhari Esfahani M, Raza A, Al Harthi S, Ebrahimi Shahmabadi H, Alavi SE. Mesoporous silica nanoparticles: synthesis methods and their therapeutic use-recent advances. J Drug Target. 2021;29(2):131-54. doi: 10.1080/1061186X.2020.1812614, PMID 32815741.
17. Sábio RM, Meneguin AB, Martins dos Santos AM, Monteiro AS, Chorilli M. Exploiting mesoporous silica nanoparticles as versatile drug carriers for several routes of administration. Micropor Mesopor Mater. 2021;312:110774. doi: 10.1016/j.micromeso.2020.110774.
18. Maleki A, Kettiger H, Schoubben A, Rosenholm JM, Ambrogi V, Hamidi M. Mesoporous silica materials: from physico-chemical properties to enhanced dissolution of poorly water-soluble drugs. J Control Release. 2017;262:329-47. doi: 10.1016/j.jconrel.2017.07.047, PMID 28778479.
19. Musallam AA, Mahdy MA, Elnahas HM, Aldeeb RA. Optimization of mirtazapine loaded into mesoporous silica nanostructures via Box-Behnken design: *in vitro* characterization and *in vivo* assessment. Drug Deliv. 2022;29(1):1582-94. doi: 10.1080/10717544.2022.2075985, PMID 35612286.
20. Abd-Elrahman AA, El Nabarawi MA, Hassan DH, Taha AA. Ketoprofen mesoporous silica nanoparticles SBA-15 hard gelatin capsules: preparation and *in vitro/in vivo* characterization. Drug Deliv. 2016;23(9):3387-98. doi: 10.1080/10717544.2016.1186251, PMID 27167529.
21. Dening TJ, Taylor LS. Supersaturation potential of ordered mesoporous silica delivery systems. Part 1: Dissolution performance and drug membrane transport rates. Mol Pharm. 2018;15(8):3489-501. doi: 10.1021/acs.molpharmaceut.8b00488, PMID 29985627.
22. Le TT, Elzhry Elyafi AK, Mohammed AR, Al-Khattawi A. Delivery of poorly soluble drugs via mesoporous silica: impact of drug overloading on release and thermal profiles. Pharmaceutics. 2019;11(6):269. doi: 10.3390/pharmaceutics11060269, PMID 31185610.
23. Budiman A, Aulifa DL. Encapsulation of drug into mesoporous silica by solvent evaporation: A comparative study of drug characterization in mesoporous silica with various molecular weights. Heliyon. 2021;7(12):e08627. doi: 10.1016/j.heliyon.2021.e08627, PMID 35005278.
24. Sreeharsha N, Rajpoot K, Tekade M, Kalyane D, Nair AB, Venugopala KN, *et al.* Development of metronidazole loaded chitosan nanoparticles using QbD

approach—A novel and potential antibacterial formulation. Pharmaceutics. 2020;12(10):920. doi: 10.3390/pharmaceutics12100920, PMID 32992903.

25. Nair AB, Shah J, Al-Dhubiab BE, Jacob S, Patel SS, Venugopala KN, *et al*. Clarithromycin solid lipid nanoparticles for topical ocular therapy: optimization, evaluation, and *in vivo* studies. Pharmaceutics. 2021;13(4):523. doi: 10.3390/pharmaceutics13040523, PMID 33918870.
26. Gomaa E, Attia MS. Ghazy FE din, Hassan A, Hasan AA. Pump-free electrospraying: A novel approach for fabricating Soluplus®-based solid dispersion nanoparticles. J Drug Deliv Sci Technol. 2021:103027.
27. Shah H, Nair AB, Shah J, Bharadia P, Al-Dhubiab BE. Proniosomal gel for transdermal delivery of lornoxicam: optimization using factorial design and *in vivo* evaluation in rats. Daru. 2019;27(1):59-70. doi: 10.1007/s40199-019-00242-x, PMID 30701460.
28. Shah PJ, Patel MP, Shah J, Nair AB, Kotta S, Vyas B. Amalgamation of solid dispersion and melt adsorption techniques for augmentation of oral bioavailability of novel anticoagulant Rivaroxaban. Drug Deliv Transl Res. 2022;12(12):3029-46. doi: 10.1007/s13346-022-01168-9, PMID 35467325.
29. Chaudhary S, Nair AB, Shah J, Gorain B, Jacob S, Shah H, *et al*. Enhanced solubility and bioavailability of dolutegravir by solid dispersion method: *in vitro* and *in vivo* evaluation-A potential approach for HIV therapy. AAPS PharmSciTech. 2021;22(3):127. doi: 10.1208/s12249-021-01995-y, PMID 33835317.
30. Jhaveri M, Nair AB, Shah J, Jacob S, Patel V, Mehta T. Improvement of oral bioavailability of carvedilol by liquisolid compact: optimization and pharmacokinetic study. Drug Deliv Transl Res. 2020;10(4):975-85. doi: 10.1007/s13346-020-00734-3, PMID 32124413.
31. Swar S, Máková V, Stibor I. Effectiveness of diverse mesoporous silica nanoparticles as potent vehicles for the drug L-dopa. Materials (Basel). 2019;12(19). doi: 10.3390/ma12193202, PMID 31574906.
32. Huang X, Young NP, Townley HE. Characterization and comparison of mesoporous silica particles for optimized drug delivery. Nanomater Nanotechnol. 2014;4:2.
33. Attia MS, Hassaballah MY, Abdelqawy MA, Mohamed ME, Farag AK, Negida A, *et al*. An updated review of mesoporous carbon as novel drug delivery system. Drug Dev Ind Pharm. 2021;(just-accepted):1-11.
34. Attia MS, Yahya A, Monaem NA, Sabry SA. Mesoporous silica nanoparticles: their potential as drug delivery carriers and nanoscavengers in Alzheimer's and Parkinson's diseases. Saudi Pharm J. 2023;31(3):417-32. doi: 10.1016/j.jsps.2023.01.009, PMID 37026045.
35. Alwan RM, Raja NA, Alhagiesa AW. Formulation and optimization of lyophilized selexipag nanocrystals to ımprove the saturation solubility and dissolution rate. Syst Rev Pharm. 2020;11(11):596-605.
36. Villalva N, Cante I, Aybar M, Rodriguez A, Torres AG, Kantor H, *et al*. Solid state forms of selexipag; 2019.
37. Voycheva CT, Tzankov B, Tzankova DG, Avramova KI, Yoncheva KP. Formulation of tablets containing glimepiride-loaded mesoporous silica particles. Indian J Pharm Sci. 2019;81(3):483-8. doi: 10.36468/pharmaceutical-sciences.533.
38. Meynen V, Cool P, Vansant EF. Verified syntheses of mesoporous materials. Micropor Mesopor Mater. 2009;125(3):170-223. doi: 10.1016/j.micromeso.2009.03.046.
39. Vazquez NI, Gonzalez Z, Ferrari B, Castro Y. Synthesis of mesoporous silica nanoparticles by sol–gel as nanocontainer for future drug delivery applications. Boll Soc Esp Ceram Vidr. 2017;56(3):139-45. doi: 10.1016/j.bsecv.2017.03.002.
40. Yu J, Shen A, Cao Y, Lu G. Preparation of Pd-diimine@SBA-15 and its catalytic performance for the Suzuki coupling reaction. Catalysts. 2016;6(12):181. doi: 10.3390/catal6120181.
41. Jia T, Zhang S, Tang S, Xin D, Zhang Q, Zhang K. Pore structure and adsorption characteristics of maceral groups: insights from centrifugal flotation experiment of coals. ACS Omega. 2023;8(13):12079-97. doi: 10.1021/acsomega.2c07876, PMID 37033861.

Cite this article: Attia MS, Ghazy FES. Ameliorating the Poor Dissolution of Selexipag in Aqueous Acidic Conditions Following Confinement into Mesoporous Silica Nanoparticles. Indian J of Pharmaceutical Education and Research. 2023;57(4):1002-11.